J. Korean Earth Sci. Soc., v. 36, no. 5, p. 419–426, September 2015
http://dx.doi.org/10.5467/JKESS.2015.36.5.419
ISSN 1225-6692 (printed edition)
ISSN 2287-4518 (electronic edition)

High Dispersion Spectra of the Young Planetary Nebula NGC 7027

Siek Hyung*, Seong-Jae Lee, and Jang-Hee Bok

Department of Earth Science, Chungbuk National University,
Chungdae-ro Seowon-Gu, Cheongju 28644, Korea

Abstract: We investigated the high dispersion spectra that had been secured at the center of the planetary nebula NGC 7027 with the Bohyunsan Optical Echelle Spectrograph (BOES) on October, 20, 2009. We analyzed the forbidden lines of [OI], [SII], [OII], [NII], [ClIII], [ArIII], [OIII], [ArIV], [NeIII], [ArV], and [CaV] in the 3770-9225Å wavelength region. The expansion velocities were derived from double Gaussian line profiles of the emission lines, after eliminating the subsidiary line broadening effects. The radial variations of the expansion velocities were obtained by projecting the derived expansion velocities: 19.56-31.93 kms $^{-1}$ onto the equatorial shell elements of the inner and the outer boundaries of the main shell of 2.5(2.1)" and 3.8(3.6)", according to the ionization potential of each ion. Analysis of equatorial shell spectra indicated that the equatorial shell generally expands in an accelerated velocity mode, but the expansion pattern deviates from a linear velocity growth with radial distance. NGC 7027, of which age is about 1000 years or less, might be still at its early stage. During the first few hundred years, plausibly in its early stage, the main shell of PN expands very slowly and, later, it gradually gain its normal expansion speed.

Keywords: interstellar matters, planetary nebulae: individual (NGC 7027), forbidden line, kinematics

1. Introduction

A planetary nebula (PN) represents a final stage of a stellar evolution that left the asymptotic giant branch (AGB) stage and will evolve into a white dwarf star in a few 10,000 years. NGC 7027 is known as a high excitation and very young PN (Aller, 1954). It is one of a few objects whose distances are accurately derived (Masson, 1989). Its age is believed to be about 1000 yr or less since it left the asymptotic giant branch phase. It is one of the brightest planetary nebulae (PNe) in the sky. Fig. 1 shows the infrared (IR) image of NGC 7027 taken trough the Hubble Space Telescope, where one clearly identifies the central star of the PN(CSPN), the bright rim (optically prominent main shell), and the outer faint halo zone. The elliptical shape bright rim corresponds to the optically bright main shell, while the outer faint halo zone can be seen only in the IR wavelength (Latter et al., 2000). The main shell seen in the bright rim is believed to be consist of stratified sub-shells with different level of ionization. The inner shell is occupied with high excitation line emissions. while the outer shell shines by low excitation lines. Unlike the HI recombination lines that occupy the whole HII region, each forbidden line represents relatively a specific narrow zone. To study the stratified sub-shell structure, it would be ideal to secure nebular specific line images for all the available forbidden line emissions. However, most emission lines are too faint to register the signal on a CCD. Hence, one must investigate the line spectra without such spectral line images.

Many authors derived the expansion velocity of NGC 7027. Some studies were done, based on mid-dispersion spectra, e.g., Sabaddin (1984) and others carried out based on medium or high dispersion spectra. However, even the most recent studies were done, based on only for a few lines. For example, Baines et al. (2003) derived an expansion velocity,

*Corresponding author: hyung@chungbuk.ac.kr
Tel: +82-43-261-2726
Fax: +82-43-271-0526

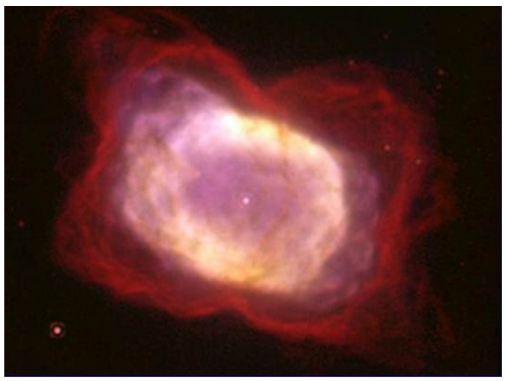

Fig. 1. NICMOS IR composite image of NGC 7027 obtained with Hubble Space Telescope. The image shows the CSPN, the bright rim (2.15 μm continuum), and the outer faint halo (2.12 μm H_2 emission. Latter et al., 2000).

13±1 km s^{-1} from [OIII] lines that represents the intermediate excitation region. Others also measured the expansion velocities in other wavelengths, for example, 19.5 km s^{-1} in the HIBrγ at 2.167 μm (Cox et al., 2002), 18.9 km s^{-1} in optical lines (Walsh et al., 1997), and 212 km s^{-1} (Ershov and Berulis, 1989). Fong et al. (2006) derived the expansion velocity of 13-16 km s^{-1} in the CO shell, while Cox et al. (2002) found an evidence of 55 km s^{-1} from the line widths in the photo-dissociation region along the bipolar axis. Such results derived by the earlier studies seem to disobey the general law for lines formed near the central star, such as [ArIV]: such high excitation lines usually march out slowly but those emitted in the outer zones, such as [N II], expand swiftly.

The expansion velocity study results have been a base for a further detailed investigation, such as distance determination, nebular shaping simulation, and kinematics studies. Unlike symbiotic stars (see e.g., Lee et al., 2012; Hyung, 2014), PNe (Lee and Hyung, 2007) show numerous forbidden lines that are useful for a velocity field study. In this investigation, we will newly derive the expansion velocity of the main shell from all the available forbidden lines secured at the center of NGC 7027 image with Bohyunsan Optical Echelle Spectrograph (BOES), hoping that the results will become a basis for a future shaping study.

The expansion velocity derivation along the major axis involves geometrical uncertainty due to the unknown projection angle, while such a projection problem does not exist in the spectra taken along the minor axis. We analyze the high dispersion spectra in the 3700-9225Å wavelength range secured at the central position of the PN, which will give the kinematical information of the equatorial shell. We will see if there is any systematic variation of expansion velocities derived from various forbidden lines observed in the optical wavelengths.

2. Observations

The spectroscopic observation was carried out on Oct. 20, 2009 (UT), with the BOES attached to the 1.8m optical telescope at the Bohyunsan Optical Astronomy Observatory (BOAO). The seeing was relatively poor, ~2.5", so we used the fiber aperture diameter of 300 for our observation, The employed relatively large diameter fiber, that allows more light within its entrance, is useful for the observation of an extended object or a point source when the weather is not good. The exposed times are 120 and 2400 sec.

2.1. data reduction and line profile analysis

We obtained two exposures, 120 and 2400 sec, on Oct. 20, 2009 (UT), with the fiber-fed Bohyunsan Optical Echelle Spectrograph (BOES) attached to the 1.8 m optical telescope at the Bohyunsan Optical Astronomy Observatory (BOAO). The seeing was relatively poor, ~2.8". We placed a 300 μm fiber entrance at the CSPN position of the PN. This fiber entrance size corresponds to a spatial resolution of 2.9" on the sky and a wavelength dispersion of R= $\frac{\lambda}{\Delta\lambda}$ =45,000.

During the observing run, we also obtained a standard-star exposure for flux calibration (58 Aql), a Th-Ar arc lamp to set wavelengths, and dome-quartz lamp exposures to fix pixel-to-pixel sensitivity fluctuation. The spectra were reduced using the IRAF echelle reduction package, following the standard procedure of bias subtraction, aperture extraction, flat-fielding, wavelength calibration, and flux calibration (Hyung,

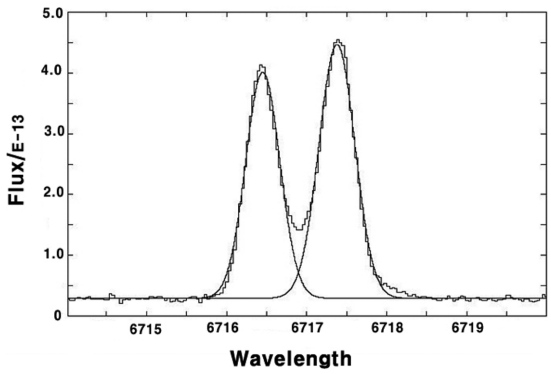

Fig. 2. [S II] 6716.47Å line profile. Exposure=40 min.

1994).

We then checked the correction factors of the Earth motion relative to the Sun with a 'rvcorrect' task in IRAF for 120 and 2400 sec, and found V_{helio}= −12.96 and −12.93 km s^{-1}. The derived heliocentric velocity corrections were applied to all of the lines, e.g., –0.28 Å for [NII] 6848. After applying these corrections, we analyze the line spectra.

2.2. Line profile and shell expansion velocity

Figure 2 shows the line profile of [S II] 6716Å that consists of double Gaussian components. We used the longer exposure of 40 min for the analysis of weak lines, while we used the shorter exposure of 2 min for strong lines, such as [OIII] 5007Å.

One can determine the shell expansion velocity from either two peaks or a full width at half maximum (FWHM), Hyung et al. (2014) describes the detailed method with an illustration on how to derive the expansion velocities from the FWHMs. The former two peaks will give the average expansion velocity of the shell, while the FWHM value will give the expansion velocity of the faster outer boundary of each stratified sub-shell responsible. In both cases, one must first eliminate the subsidiary broadening factors except for the shell expansion component itself.

The main structure of NGC 7009 can be described as an ellipsoidal shell filled with gases of ionized hydrogen (HII) and other ions that consists of multiple layers of different electron temperatures (Aller, 1956). Since the HI recombination emission gases occupy the whole shell, one cannot peel off the multiple layers of kinematically different sub-shell. Hence, instead of using H lines, we employed all the other available forbidden lines to differentiate the stratified sub-shell structures. Each forbidden line is likely to be formed with a specific sub-shell of different physical condition. We did not either use the HeI and HeII lines for our study for the same reason mentioned as in the hydrogen case.

The line widths are subject to broadening due to the differential motion of the expanding shell gases or due to the axial difference of the expansion shell structure. The overall geometry of the main shell of NGC 7027 can be represented as a hollow ellipsoidal sphere. Since the observed spectral lines are secured at the center of NGC 7027 which corresponds to the equatorial shell, we assume the torus-like equatorial shell expands radially outward and we may ignore the other directional tangential movements (see 3-D model by Walsh et al., 1997). In this case, the equatorial shell observed only at the center of the image would have a cross-section of the front approaching shell and the rear receding shell. Thus, we expect a double Gaussian line profile from the observed lines secured at center of the image.

As mentioned earlier, one must eliminate other subsidiary broadening factors to find the pure expansion velocity from the measured line width, These subsidiary factors are:

(1) thermal broadening factor, $V_{th}=(8kT_e\ln 2/m)^{0.5}= 21.6\times 1.0^{-2}\times T_e\times m^{-0.5}$ km s^{-1}. Here, k is Boltzmann constant, m is atomic mass, and T_e is electron temperature in K. Literatures give various derived values, such as 17500 K (Blocker, 1995), T_e=13,500 K (and density $\log N_e$=4.7; Middlemass, 1990). We adopt T_e=13,500 K. (2) instrumental broadening factor, V_{inst}. The light from the object that pass_through various paths, such as mirrors, lenses, gratings, and a prism in the BOES system, must be considered. This instrumental broadening effect will appear in the intrinsically narrow lines, such as Th-Ar lines. We adopt V_{inst}=6.58±0.90 km s^{-1}, derived from $V_{inst}=c\times\frac{\Delta\lambda}{\lambda}$, after measuring $\Delta\lambda$ from

Table 1. Expansion velocity derivation

Ion	λ_{obs}	FWHM	V_{FWHM}	$2V_{exp}$	V_{exp}	ΔP	$V_{\Delta P}$
[OI]	5576.83	0.69	37.12	35.99	17.99	0.45	12.10
[OII]	3725.74	0.83	66.83	66.21	33.11	0.52	20.93
	3728.49	0.85	68.39	67.78	33.89	0.53	21.32
	7318.96	1.57	64.15	63.50	31.75	1.04	21.31
			mean:	32.91±0.88		21.19±0.18	

Velocity unit: km s^{-1}. V_{th}=6.27. V_{inst}=6.59. V_{turb}=5 (forbidden). The last row gives the mean values, V_{exp} and $V_{\Delta P}$ with standard deviation errors, 0.88 and 0.18 km s^{-1}, respectively. ΔP: Å.

several Th-Ar line widths. (3) turbulence broadening factor, $V_{f\text{-}s}$. The forbidden lines are formed due to collisions with electrons passing by. This factor is known to be relatively small. We assume $V_{f\text{-}s}$=5 km s^{-1} (Sabbadin et al., 2006). Then, we can derive the expansion velocity from the relation, $V^2_{FWHM} = 2V^2_{exp} + V^2_{th} + V^2_{inst} + V^2_{turb}$ or $2V^2_{exp} = V^2_{FWHM} - V^2_{th} - V^2_{inst} - V^2_{turb}$.

To show the derivation procedure, we list the measured wavelength widths and derived expansion velocities for [OI] and [OII] lines in Table 1. Successive columns list ions, observed wavelengths, FWHM(Å), $2V_{exp}$, V_{exp}, ΔP(Å), and $V_{\Delta P}$. The ΔP is the wavelength difference between two peaks of a double Gaussian line profile. The detailed explanations on how to measure the FWHM from the double Gaussian line profile are given in Hyung et al. (2014). Two forbidden lines, [OI] and [OII], give mean values of V_{exp} as 17.99 and 32.91±0.88 km s^{-1}, respectively, while they give $V_{\Delta P}$ as 12.10 and 21.19±0.18 km s^{-1}, respectively. The former V_{exp}s are about 1.49 and 1.55 times larger than the latter $V_{\Delta P}$s.

We also derived the expansion velocities for other forbidden ions in a similar way. The estimated errors in deriving velocities are mostly about 0.88 km s^{-1} (indicated by [OII] lines in Table 1). The errors are likely to be slightly larger for the weaker lines, such as [ArV], but smaller for the stronger lines, such as [OIII]. Table 2 lists all the available expansion velocities. The CSPN temperature of NGC 7027 is known to be high, reaching about 200,000K (Latter et al., 2000). The hot CSPN ionizes the surrounding gases in a shell which can be seen in a (stratified) multiple sub-shell structures of forbidden lines. Column (2) lists the ionization potential (IP) of each ion. Columns (3) and (4) the expansion velocities (V_{exp}) by us and the earlier determination by Sabbadin (1984). The high excitation emission lines from highly ionized ions, such as [ArV], occupy the inner zone, while those from lowly ionized ions, such as [SII] and [NII], occupy the outer part. Hence, we list the expansion velocities in the descending order of the IPs.

In general, the expansion velocities for the high excitation lines that have been formed in a zone close to the CSPN, are generally smaller than those for the low excitation lines in the outer zone. Unfortunately, there is no way of determining the radial distance of the emission zone from the CSPN based on the observed images: The narrow band filter or line images, which define the spatially resolved regions, are not available except for the strong line like [OIII]. Hence, we employed an alternative way of inferring the radial distance of the emission zone based on the IP of each ion. Here, we assume that the radial distances of ions are inversely proportional to their IP values. The highest IP line, such as [Ca V], should be located at an inner zone near the inner boundary of the main shell, while the lowest IP line, such as [S II], is expected be located at the outer boundary. We ignored the result of the [OI] line, since this neutral line is believed to be formed sparsely in the high density neutral blobs of PN (Osterbrock, 1989).

Once the inner and outer boundaries of the main shell are given, we are able to assign each emission line to a specific radial distance, within the main shell according to each IP value. Based the 1.4 GHz contour images, Bains et al. (2003) defined the dimension of the main shell as about 7.2"×11.5", in the minor and major axes. This would set the outer radius of the

Table 2. Expansion velocities

Ion	IP(eV)	V_{exp}	S84	r(")
[OI]	0.0	17.99	22.75	
[SII]	10.4	31.93	21.35	(3.60)
[OII]	13.6	32.91	23.6	(3.52)
[NII]	14.5	30.89	20.8	(3.50)
[CIIII]	23.8	-		
[ArIII]	27.6	29.57		(3.14)
[OIII]	35.5	27.54		(2.94)
[ArIV]	40.7	19.95		(2.80)
[NeIII]	41.0	-	22.35	
[ArV]	59.8	21.00		(2.29)
[CaV]	67.1	19.56		(2.10)

S84: from Sabbadin (1984). r("): projected radial distances according to IPs with the shell boundaries of 2.1"-3.6". See the text for discussions on other boundaries, Δr=2.3"-3.6" and Δr=2.5"-3.8".

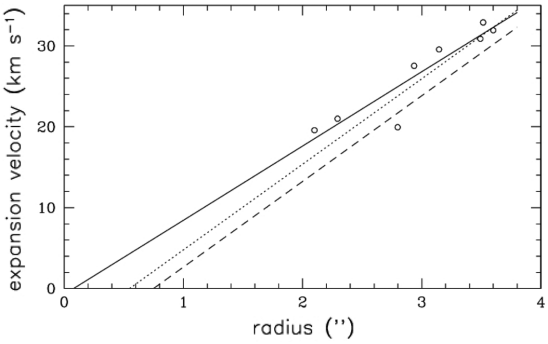

Fig. 3. Expansion velocities V_{exp} (km s^{-1}) vs. radius (in arc-sec). The radii of ions have been calculated based on the IPs, inversely proportional to their values. The solid line and the open circles are for the data with the shell boundary of Δr=2.1"-3.6". dotted line: refitting with Δr=2.3"-3.6". dashed line: refitting with Δr=2.5"-3.8". See the text.

equatorial shell as r=3.6". The HST WFPC2 optical image, however, seems to indicate the boundary determination is not an easy job. The structure of the main shell responsible for the bright rim seems much more complicated than the radio or the infrared data suggested. We also referred to the NICMOS 2.15 HI continuum image which defines the inner and outer boundaries of the bright rim fairly well.

First, we start with the above 3.6" as an inner boundary radius and we further assume that the radius of the inner boundary to be 0.58 times that of the outer boundary, i.e., 2.1" (see Fig. 1). The last column of Table 2 lists the radial distances (in seconds of arc) determined according to this assumption. The results are plotted as open circles in Fig. 3. The solid line gives a linear fit to the data. Except for [NII] and [ArIV], most data are aligned close to this solid trend line, implying a simple linear relationship between the differential expansion velocities and the radial distances exists which goes down to the CSPN position, ~0 km s^{-1} at 0pc. Hence, it indicates that the expansion velocity of each sub-shell linearly increases with radial distance from the CSPN. The expansion velocities derived by us or Sabaddin (1984) are for the main shell. Meanwhile, Sabbadin (1984) could not find any trend from their study. The present study clearly shows a linear relation of increasing expansion velocity alow with the radial distance. This first fitting implies that the so-called Hubble type flow character is present in NGC 7027.

Although our data show a systematic variation that was not present in the result by Sabbadin (1984), a large scatter exists in [ArIV]. We do not know whether this is due to an error or a genuine factor present in the line emission zone. Note that the derived expansion velocity values are very different from those for the CO shell or photo-dissociation region. The CO or photo-dissociation emissions are prominent mostly along the bipolar axis (Fong et al., 2006; Cox et al., 2002). The kinematics of the major axis or the overall geometry involving the outer halo molecular zone is beyond the present study. Hence, we will avoid any further discussion.

Note that we derived two different expansion velocities, V_{exp} and $V_{\Delta P}$. The former may correspond to the highest value of each line emission shell, while the latter must represent the middle position or the mean value of the same stratified shell. If so, the expansion velocity of the high excitation [CaV] line given in Table 2, would not represent the inner shell boundary, 2.1". Hence, we considered the sub-shell thickness responsible for this [CaV] (and other lines) and we adjusted the radial distances slightly outward, for most lines except for the lowest excitation line, [SII], at the outer boundary. At first, we assume that

all the sub-shells have the same thickness of 0.3". Then, we assigned each expansion velocity value to a specific radius within the main shell boundaries, Δr= 2.3"- 3.6".

We performed another job of additional fitting with new boundaries. The additional trend line is also plotted in Fig. 3 (see the dotted line) This second results seem rather surprising: the extrapolation of the trend line does not go back to a zero point, i.e., below V_{exp}=0 km s^{-1} at the CSPN surface.

With slightly larger boundary values, r=2.1"-3.8" and with a slightly increased sub-shell thickness of 0.4" (that is, velocity data points fall into a region of shell boundaries Δr=2.5"-3.8"), we thirdly performed another fitting job. This time, we found about the same result, but the deviation from the data points is larger compared with the first linear fit (see the dashed line in Fig. 3). Among three, the third one with a larger shell thickness seems most appropriate, considering the HST optical images or Keck HIRES spectral images (unpublished data by Hyung et al., 2015). The acceleration in the expansion velocity seems to exist in the equatorial shell, but it does not follow a Hubble type expansion.

Once the distance to PN, such as 0.98 kpc, by 4.9 GHz radio flux maps by Zijlstra et al. (2008), is given, one can use the actual size of the equatorial shell or each sub-shell radius (in pc) from the CSPN responsible for the emissions. We do not list all the radii in Table 2 since the present study is based on a simple assumption for physical parameters. Before processing any further study with the physical parameter, one must, in fact, fully investigate the characteristics of kinematics hidden in the derived expansion velocities.

A while ago, Walsh et al. (1997) introduced a linear velocity law in their three-dimensional (3D) field of NGC 7027 shell,

$$V = -10+1400\frac{r(pc)}{D(kpc)},$$

where r is the radial distance from the CSPN and D is the distance. The peak velocities, V_{minor} and V_{major}, reach 14.5 and 29 km s^{-1} on the minor and major axes, respectively. Zijlstra et al. (2008), however, pointed out that the velocities adopted by this 3D model cannot match the presently observed nebular shaping. The afore-mentioned maximum velocity (14.5 km s^{-1}) of the equatorial shell by Walsh et al. (1997) are smaller than the value indicated by our [OII] results, V_{exp}=31.93 km s^{-1} or $V_{\Delta P}$= 21.18 km s^{-1}. One might improve the above mis-matching problem with our data.

The Chandra X-ray satellite observation shows the bipolar X-ray emission of T_{eff}~1000,000K in the main shell (Kastner et al., 2001). Apparently, NGC 7027 just experienced the first few hundred years of kinematically unstable phase, right after leaving its AGB phase. The equatorial region of the main shell are now gradually approaching the physically stable status.

3. Conclusions

We analyzed the high dispersion spectra of forbidden lines secured at the central position of the young PN NGC 7027. The spectral lines enable us to derive the expansion velocity of the equatorial shell. The expansion velocities deviate from a linearity of the Hubble type acceleration: the observed velocity does not start with V_{exp}=0 km s^{-1} (but below 0) at the center r=0 (see the second or third fitting in Fig. 3). This trend line is quite strange, since one expects a high speed ejection due to the stellar wind from the relatively high temperature CSPN.

Recently, Hyung et al. (2014) carried out a similar study on the equatorial zone of the saturn type PN NGC 7009. The more evolved PN NGC 7009 shows an opposite trend in its equatorial part of the main shell, i.e., V_{exp}~20 km s^{-1} at r=0 pc. In any normal PN, the stellar radiation pressure of the pre-PN would push away the detached shell gas and dust shell, so they must reach at a certain terminal velocity, at least, of a few km s^{-1} within a few decades (Castor et al., 1981). The halo zone of NGC 7009 and probably NGC 7027, which might be the earlier AGB ejecta, does

not seem suffering a problem of deviation from a Hubble type expansion. The outer halo zones seem to start expanding with V_{exp}~0 km s^{-1} at r=0 pc.

NGC 7027 is very young, probably its age of less than 1000 years. Hence it might be still at an early stage of its shaping. Perhaps in its the early stage during the first few hundred years after its AGB phase, the main shell of PN expands very slowly, and in the later stage it gains its normal expansion speed. Probably we are currently witnessing such an evolutionary change. At this stage, the central star temperature might be lower than the later, i.e., present time. Such a situation, however, cannot be accommodated by concurrent theoretical evolutionary track models (Blocker 1995; Natta and Hollenbach 1998).

There is an alternative explanation for the physical parameter of the main shell at the beginning phase of PN based on our study. Other studies report that the expansion velocity of the polar zone observed along the major axis is faster that of the equatorial zone along the minor axis (Walsh et al. 1997). The retarded expansion velocities in the equatorial zone found by the present study might be due to a large amount of dust in the equatorial shell region in the earlier evolutionary stage of NGC 7027. The dust might reduce the expansion motion along the equatorial shell for the last few hundred years. The circumstellar dust might be responsible for the slow expansion of the equatorial gas shell. In fact, there are several IR observational studies, which confirmed a large amount of dust in NGC 7027. This topic is beyond the scope of the present study.

In conclusion, the linear relationship of expansion velocities with radius, proposed in the 3D model by Walsh et al.(1997) does not seem to hold for NGC 7027. As pointed out by Zijlstra et al. (2008), NGC 7027 is at an early phase of the evolution, which might eventually evolve into an X shape morphology. In the early pre-planetary evolutionary phase, the physical condition of the CSPN and the main shell of NGC 7027 must be quite different from those observed today. In future study, one must consider a non-linear time dependent velocity model to simulate the evolutionary shaping of NGC 7027.

Acknowledgment

This work was supported by the research grant of Chungbuk National University in 2014. We would like to acknowledge support from the Basic Science Research Program through the National Research Foundation of Korea (NRF 2014R1A1A4A01006509; NRF 2015R1D1A3A01019370).

References

Aller, H.L., 1954, The composition of the planetary nebula NGC 7027, Astrophysical Journal, 120, 401-411.

Aller, H.L., 1956, Chemical compositions of selected planetary nebulae, Astrophysical Journal, 125, 84-100.

Bains, I., Bryce, M., Mellema, G., Redman, M.P., and Thomasson, P., 2003, High-resolution radio structure and optical kinematics of NGC 7027, Monthly Notice of the Royal Astronomical Society, 340, 381-397.

Blocker, T., 1995, Stellar evolution of low- and intermediate-mass stars. II. Post-AGB evolution, Astronomy and Astrophysics, 299, 755-769.

Castor, J.I., Lutz, J.H., and Seaton, M.J., 1981, Ultraviolet spectra of planetary nebulae. III - Mass loss from the central star of NGC 6543, Monthly Notices of the Royal Astronomical Society, 194, 547-567.

Cox, P., Huggins, P. J., Maillard, J.-P., Habart, E., Morisset, C., and Bachiller, R., 2002, High resolution near-infrared spectro-imaging of NGC 7027, Astronomy & Astrophysics, 384, 603-619.

Ershov, A. A. and Berulis, I. I., 1989, Radio Recombination Lines and the Expansion Velocity of the Planetary Nebula NGC7027, Soviet Astronomy Letters, 15, p178.

Fong, D., Meixner, M., Sutton, E. C., Zalucha, A., and Welch, W. J., 2006, Evolution of the Circumstellar Molecular Envelope. I. A BIMA CO Survey of Evolved Stars, The Astrophysical Journal, 652, 1626-1653.

Hyung, S., 1994, Density contrast shell models for the planetary nebula IC 2165, Astrophysical Journal Supplement Series, 90, 119-148.

Hyung, S., 2014, Spectroscopic Study of the Symbiotic Star CI Cyg, Journal of Korean Earth Science Society, 35, 313-323.

Hyung, S., Lee, S-J., and Sung, E., 2014, Expansion velocities of the planetary nebula NGC 7009°™the high dispersion spectra line profiles, Astrophysics and Space

Science, 352. 71-81.

Hyung, S. and Lee, S-J., 2015, in preparation.

Kastner, J.H., Vrtilek, S.D., and Soker, N., 2001, Discovery of Extended X-ray Emission from the Planetary Nebula NGC 7027 by the Chandra X-ray Observatory, The Astrophysical Journal, 550, L189-L192.

Latter, W.B., Dayal, A., Bieging, J.H., Meakin, C., Hora, J.L., Kelly, D.M., and Tielens, A.G.G.M., 2000, Revealing the Photodissociation Region: HST/NICMOS Imaging of NGC 7027, The Astrophysical Journal, 539, 783-797.

Lee, S. J., Hyung, S., and Lee, K.W., 2012, An Analysis of the Symbiotic Star Z and Line Profile, Journal of Korean Earth Science Society, 33, 608-617 (in Korean).

Lee, S. M. and Hyung, S., 2007, Kinematics and Geometrical Structure of the Planetary Nebula NGC 6881, Journal of Korean Earth Science Society, 28, 847-856 (in Korean).

Masson, R.C., 1989, The structure of NGC 7027 and a determination of its distance by measurement of proper motions, Astrophysical Journal, 336, 294-303.

Middlemass, D., 1990, A model for the planetary nebula NGC 7027. Monthly Notice of the Royal Astronomical Society, 1990, 294-309.

Natta, A. and Hollenbach, D., 1998, The evolution of the neutral gas in planetary nebulae: theoretical models, Astronomy and Astrophysics, 337, 517-538.

Osterbrock, D.E. 1989, The Astrophysics of gaseous nebulae and Active Galactic Nuclei, University Science Books (Mill Valley, CA, 1989).

Sabbadin, F., 1984, A catalogue of expansion velocities in planetary nebulae, Astronomy & Astrophysics Supplement Series, 58, 273-285.

Sabbadin, F., 2006, The structure of planetary nebulae: theory vs. practice, Astronomy and Astrophysics, 451, 937-949.

Walsh, J. R., Dudziak, G., and Walton, N. A., 1997, Modelling the expansion of NGC 7027, In IAU Symp. 180, Planetary Nebulae, ed. Habing & Lamers (Dordrecht: Kluwer), p 286.

Zijlstra, A.A., van Hoof, P.A.M., and Perley, R.A., 2008, The Evolution of NGC 7027 at Radio Frequencies: A New Determination of the Distance and Core Mass, Astrophysical Journal, 681, 1296-1309.

Manuscript received: July 31, 2015
Revised manuscript received: September 16, 2015
Manuscript accepted: September 18, 2015